Spring 5-17-2019

Nuclear Magnetic Resonance Characterization of Dynamics in Novel Electrochemical Materials

Christopher T. Mallia
CUNY Hunter College

Nuclear Magnetic Resonance Characterization of Dynamics in Novel Electrochemical Materials.

by

Christopher Mallia

Submitted in partial fulfillment
of the requirements for the degree of
Master of Arts in Physics, Hunter College
The City University of New York

2019

Thesis Sponsor: Steve Greenbaum

May 16th, 2019	Steve Greenbaum
Date	Signature
May 16th, 2019	Phil Stallworth
Date	Signature of Second Reader

ABSTRACT

Advisor: Steve Greenbaum

As our daily use of electronics and electronic technology grows, so does the societal need for sustainable, renewable and portable electrical power. To this end, materials of interest in the electrochemical world are needed to advance the frontier of battery science and energy storage technologies so that a safer, more efficient and reliable electrical future can be realized. This work focuses on characterization of materials primarily of interest for use as electrolytes in rechargeable Lithium-Ion Batteries (LIBs). Despite their extraordinary power, LIB application in certain fields, such as in electric vehicles, has been limited due to performance and safety concerns. It is to overcome this barrier that the efforts of characterization studies such as this are needed, so that the next generation of batteries can perform reliably and safely in all applications. In this work the dynamics of a novel solid polymer electrolyte are discussed, and their disruptive implications on the battery industry. A system of Ionic Liquids (ILs) which are candidate electrolyte solvents are examined using Fast Field Cycling (FFC) NMR. A deep eutectic solvent system of glycerol-d8 and a polar salt Choline Chloride is probed using High Pressure Nuclear Magnetic Resonance (HP-NMR) studies.

For George- the most loyal friend, and curious assistant (2005-2018).

ACKNOWLEDGEMENTS

I would foremost like to thank Professor Steve Greenbaum for his constant mentorship throughout these past years, without him I would never have had the opportunity to conduct professional science as supported and comfortably as I have in his group. His guidance in all matters, scientific and personal has always been of the utmost value to me, and I can never repay the kindness he has shown me. I have learned what it means to be an invaluable and amazing scientist by his example.

I must personally thank Dr. Phil Stallworth especially, for his incredible patience and guidance as I have worked on projects through the years. His command of theory is only matched by his experimental prowess, and without his unmatched skill as an experimentalist, my work may have taken decades. I owe him not only for a profound education in science and the tools needed to do it, but also in helping me find true meaning in the work we do.

I would be remiss in not mentioning the outstanding examples of scientists I have had the pleasure of working alongside. Dr. Lisa Cirrincione, you have been my friend and mentor since I step foot in the lab, and I can never repay you for your kindness and honesty when I needed it most. Dr. Kartik Pilar, who taught me to take the good of HP-NMR with the bad, and being a sympathetic ear when it was the latter, thank you for your friendship and mentorship. Dr. Steve Muñoz, who helped my experience with both humor and wisdom as a colleague and true friend. Dan Morales, my office-mate, for his guidance and friendship.

I also need to thank all the wonderful lab members of the Greenbaum group, both past and present: Dr. Mallory Gobet, Dr. Mounesha Garega, Dr. Carla C. Fraenza, Dr. J. R P. Jayakody,

Shen, Sunita, Dave, Sahana, Nishani, Jing, Fernando, Jessica, Rachel, Bart, Maribel, Ariane, Ysaris. Thank you all for making my experience as wonderful personally as it was professionally.

Last but not least, I must thank my family; my parents, Mike and Corrine, my brother Dan and his wife May, and my love, Elina, for their constant support and foundation of happiness upon which I could build my work. Your places in my life are unfaltering, and I cannot have done anything without you. Further in memory of my grandfather, Joseph: veteran, engineer and CCNY alum, for imparting his stubborn and skeptical pursuit of truth onto me. Thank you always.

Table of Contents

List of Figures

Chapter 1: Batteries and Constituent Components

1.1 Introduction to Energy Storage

Electrical storage devices take the form of batteries, capacitors and inductors, as well as a few more exotic devices. Capacitors and Inductors store electrical energy in the form of electric and magnetic fields, respectively. Unlike capacitors and inductors, which tend to not retain energy storage over long lifetimes, batteries by design store energy in the form of electrochemical reactions that can be triggered at any time after being stored. These reactions are known as a redox reaction, whereby electrons are oxidized from a chemical species in the battery at the cathode, vindicating them to travel through a circuit and do work which provides electrical power, while the oxidized molecule moves in the opposite direction through the battery and is reduced at the anode. Batteries that are not capable of the reverse chemical reaction (e.g. common chemistry such as zinc-carbon) are called primary batteries, and are not rechargeable. Battery chemistries that do allow for the reverse reaction, and therefore recharging, are called secondary batteries (such as lithium-ion and their poor-performing cousin Nickel-Cadmium), and now dominate the majority of common electrical applications [1].

Demands of the electrical application in question determine the type of battery used in a device. Battery chemistries differ in voltage, discharge rate, internal resistance, and cycle performance. This work will focus on materials for use in secondary batteries, or those that are rechargeable. A battery consists of several simple idealized components: an anode; or negatively charged electrode where oxidation occurs, a cathode; a positively charged electrode where reduction occurs, an electrolyte; where a charge-carrying salt is dissolved to give the oxidized

species and free electrons, and typically a porous separator; that keeps the space in between electrodes physically filled for the liquid solvent and salt to move in, as well as restrict the flow of electrons (non-electrically conductive). Figure 1. depicts conventional battery chemistry, here representing a common lithium ion battery system.

Battery performance is of the utmost concern in applications, and several considerations are needed. Aside from the technical specifications of a battery (voltage, internal resistance), cycle performance dictates how the battery will retain charge over a lifetime of charging and discharging. Common rechargeable batteries are typically manufactured for performance over 200-1000 cycles, after which irreversible chemical reactions that can occur at the electrodes degrade performance or prevent effective charge moving in the battery [1]. These performance lifetime considerations are an important factor in determining cathode and anode materials in a battery, as well as the interface properties between the cathode and electrolyte material [2].

1.2 Structure of Lithium Ion Secondary Batteries

As mentioned in the prior section, lithium ion batteries are a secondary battery type, and consist of the same internal components discussed in that section. Common cathode materials industrially are Manganese Oxide (MnO_2), Manganese-Cobalt Oxide ($MnCoO_2$) or other transition-oxide compounds of interest [1]. Anodes are typically composed of graphite, and electrolyte chemistries can vary greatly between specific batteries. Common lithium salts include Lithium bis(trifluoromethanesulfonyl)imide (LiTFSI), Lithium hexafluorophosphate ($LiPF_6$). The choice of each of these materials can greatly affect the performance of a lithium battery, and

the resultant safety as well.

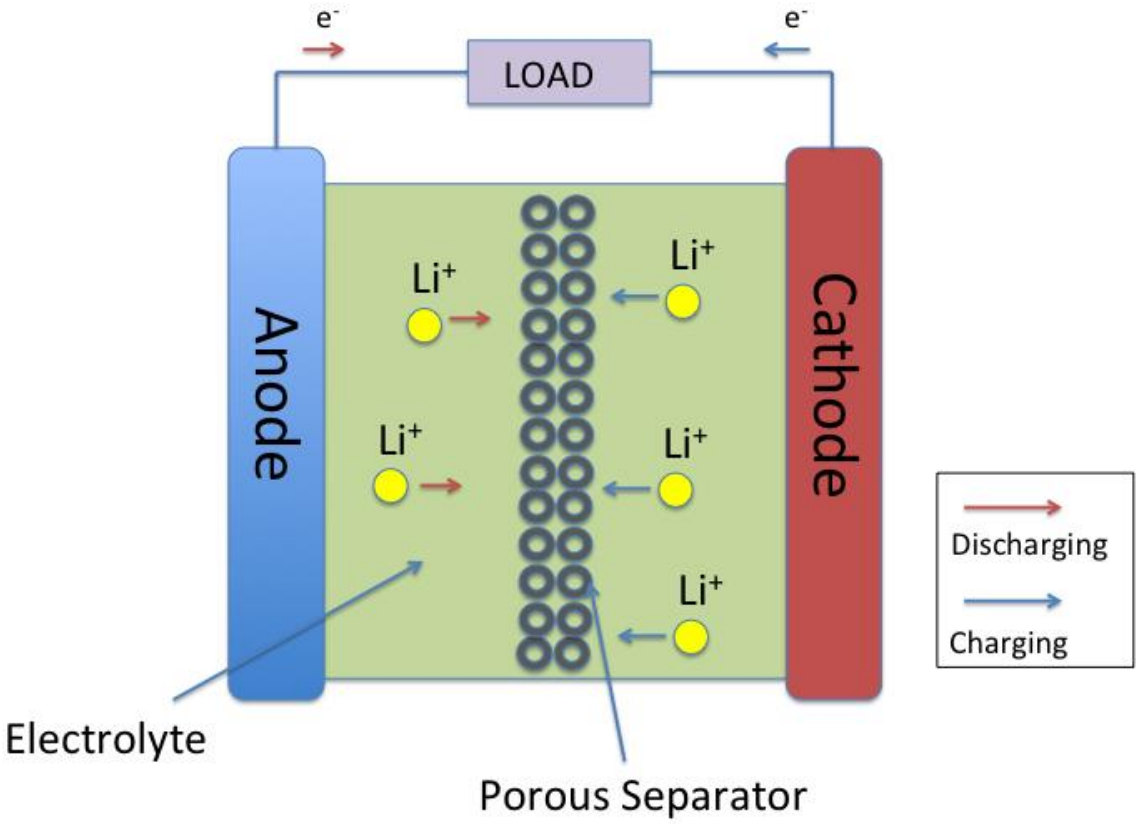

Figure 1. A schematic representation of a lithium ion secondary battery with simplified components.

The main concern that keeps lithium ion batteries away from use in large-scale electrical applications is that of safety. Commonly available lithium ion batteries typically are constructed with a flammable organic solvent, which can undergo thermal runaway should the battery be overcharged, shorted electrically, or physically damaged [1,2,3]. Yet their high energy density, long cycle life and energy efficiency as well as sustainability in comparison with other battery types have retained their favor in industry [3]. Despite this, applications in electric vehicles, planes or large-scale electric grid storage applications are usually heavily restricted because of

safety concerns. To change this, novel and unique materials must be introduced to batteries that can address these concerns.

Bringing lithium ion technology into widespread use in all applications safely is one of the objectives of research in battery science in the present [3]. These efforts mainly focus on one of several issues. The first, and foremost in this work, is to characterize and understand safe electrolyte materials in order to be comparable to those that are volatile in terms of specific capacity and conductivity. The second is to improve interfaces with the electrodes in order to avert problems such as dendrite formation, whereby lithium metal grows at the anode and shorts the battery if left unchecked. This body of research is explored in depth in many publications, with varying chemistries and mechanisms considered [4,5]. It is through the understanding of these systems and their underlying fundamental behavior that we can address the sources of failure in application. Through the mechanistic study of novel materials for these applications, we can gain insight into what would make a lithium ion battery safer and more reliable.

Chapter 2: Nuclear Magnetic Resonance

2.1 The Formalism of NMR

Nuclear Magnetic Resonance (NMR) is a technique that can be understood as the exploitation of a fundamental property of the nuclei that constitute atoms in nature. The Stern-Gerlach experiments at the beginning of the 20th century hinted at a fundamental property of nuclei that had not been previously described, that would account for phenomenological behavior in the presence of magnetic fields. In 1938, Isidor Rabi demonstrated the first instances

of a nuclei resonating in an external magnetic field [6]. NMR has since become a scientific mainstay technique for characterizing the magnetic and electrical properties of matter on a molecular level, allowing insight into dynamics of nuclei in bulk systems. Furthermore, due to the fundamental nature of nuclei, as detailed below, NMR is nuclei selective, allowing for the direct probing of systems at specific chemical sites, as well as particular species in multi-component systems.

The formalism of Quantum Mechanics tells us that the intrinsic property of a nuclei known as spin is discretized in a basis analogous to those of angular momentum. The quantum numbers in this basis obey similar quantization conditions as those of a total angular momentum, namely that the Spin (***I***) number can be non-negative half integers or integers (in units of $\hbar$). The projection of spin along an arbitrary axis taken to be in the $\hat{z}$ direction is therefore restricted to have values (in the correct units) of $\mathbf{I_z} = \mathbf{m}\hbar$, where $\mathbf{m} = -\mathbf{I}, \mathbf{-I+1}, .. \mathbf{0}, ... \mathbf{I-1}, \mathbf{I}$ (a total of $2\mathbf{I}+1$ values) and $\hbar$ is the reduced Planck constant. For typical nuclei, such as in hydrogen (^{1}H) or fluorine (^{19}F), $\mathbf{I} = {}^{1}/_{2}$. Nuclei such as in atomic Lithium (^{7}Li) have higher order spins $\mathbf{I} = {}^{3}/_{2}$. Nuclei possessing nonzero spins have a magnetic moment, and are called "NMR active" because they can interact with an external magnetic field. The magnetic moment, denoted by $\boldsymbol{\mu}$, is given by the expression:

$$\boldsymbol{\mu} = \gamma \boldsymbol{I} \qquad \textbf{[Eq. 1]}$$

where γ is the gyromagnetic ratio, a constant specific to a nuclei (in units of frequency /Tesla) , relating the strength of its magnetic moment to its intrinsic spin. Because spin is a vector quantity, the magnetic moment possesses both magnitude and direction, so considering only the

$\hat{z}$ component gives $\boldsymbol{\mu_z = \gamma I_z}$. Note that for many nuclei, with z-components of spin with **m** possible values, nuclei in a given sample can be in different spin states. While the discussion here will mainly consist of spin ½ nuclei, in general higher order transitions between values of **m** are possible, but are sufficiently suppressed.

Classical electrodynamics tells us that a magnetic moment in the presence of an external magnetic field experiences a net torque given by the expression:

$$\boldsymbol{N = \mu \times \overrightarrow{B_0}} \qquad \textbf{[Eq. 2]}$$

where $\boldsymbol{\overrightarrow{B_0}}$ is the external magnetic field (N is used here as torque to avoid confusion with the time variable τ) [7]. This same principal applies to the magnetic moments generated by nonzero nuclear spins. Therefore, in the laboratory frame, or inertial relative to the spin precession, the nucleus experiences a torque in an external magnetic field resulting in an angular precession about the magnetic field. This torque rotates the total spin around the axis of $\boldsymbol{\overrightarrow{B_0}}$ in a direction normal to the projection of the spin and to the magnetic field (clockwise or counterclockwise depending on the sign of γ). This rotation occurs at the Larmor frequency according to the relation [7]:

$$\boldsymbol{\omega_0 = \gamma B_0} \qquad \textbf{[Eq. 3]}$$

We choose in the laboratory once again to place the magnetic field along the $\hat{z}$ direction for simplicity. With this coordinate system, a visual representation of this precession is given by Figure 2.The energetic description of this rotation gives that the total energy of this precession is given by:

$$\boldsymbol{E = -\mu \cdot \overrightarrow{B_0} = -\gamma I_z B_0 = -\gamma m \hbar B_0} \qquad \textbf{[Eq. 4]}$$

known as the Zeeman energy. For two adjacent states, with **m** values separated by Δ**m**=1, the energy difference is also separated by an amount quantized by:

$$\boldsymbol{\Delta E = \gamma \hbar B_0} \qquad \textbf{[Eq. 5]}$$

From the Planck-Einstein relation $\boldsymbol{E = \omega \hbar}$, one arrives at the frequency of a photon that has an energy equivalent to this separation in Zeeman energies:

$$\boldsymbol{\omega = \gamma B_0} \qquad \textbf{[Eq. 6]}$$

We can see from comparison of Eq. 6 and Eq. 3 that the Larmor frequency of precession of the magnetic moment in the external magnetic field is the same as the frequency of a photon needed to excite a transition between adjacent values of **m**. Note that because **m** was discretized into 2**I**+1 possible values, there are an equivalent number of possible Zeeman energy levels. Therefore it is possible to excite transitions between Zeeman energy levels with the absorption of a photon of the Larmor frequency. For almost all active nuclei at fields of several Tesla magnitudes, this frequency is typically in the Radio Frequency (RF) region.

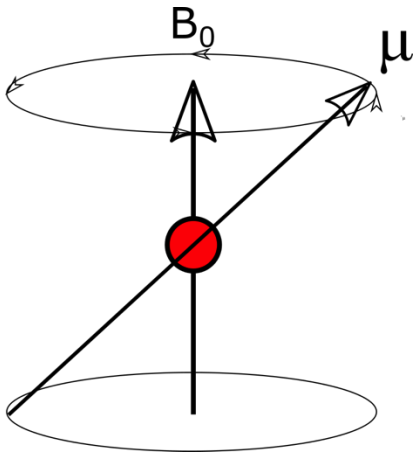

Figure 2. A visual representation of Larmor precession of a magnetic moment about an external field.

2.2 Experimental NMR Details

From an experimental point of view, the formalism presented in the previous section allows for the excitation of nuclei in an external magnetic field using radio frequency radiation. The details of delivering this radiation will be discussed further, but first a note on the practicality of experimental NMR. We see in Eq. 5 and Eq. 6 that Zeeman energy spitting, and therefore needed frequency of radiation to excite transitions is dependent on the strength of the external field. In practicality, these fields could be any nonzero value, however magnetic fields are used of order several Tesla, so that radio frequencies are the primary frequency ranges for the precession. This is chosen partially to maximize the energy difference such that higher resolution in the resultant signal, as will be discussed in a further section, can be acquired. It also coincides with well-established electronics that operate on the necessary frequency scales.

After establishing the precession of the spins of nuclei in a magnetic field, the question of delivering energy in the form of electromagnetic radiation in order to excite transitions becomes pertinent. First, we must discuss the populations of species available to be excited. In bulk samples, Avogadro's number of active nuclei may be present and contribute magnetic moments to bulk magnetization. These magnetic moments as we have seen, have several possible states in the presence of an external field. For a simple nuclei of $\mathbf{I} = {}^1/_2$ only values of $\mathbf{m} = \pm {}^1/_2$ are possible. Therefore the $\hat{z}$-projection of the nuclear spin can be aligned with the magnetic field, or anti-aligned. The anti-aligned state is energetically less probable, because it is a higher energy (the minus sign contributes to the energy of a given state in Eq. 4) state and at thermal equilibrium has a lower probability. Therefore there will be some population in either state,

which can reasonably at room temperature be represented by Boltzmann statistics for both populations. We have therefore the expression:

$$\frac{N_a}{N_b} = e^{-\Delta E/k_b T} \qquad \textbf{[Eq. 7]}$$

where population N_a describes anti-aligned states and N_b aligned states, k_b the Boltzmann constant, and T temperature in Kelvin. This population expression at room temperature and for Zeeman energy splitting at fields of order 1Tesla is in favor of the aligned states only by a small amount, hence the important need of high magnetic field strengths. The available difference in the aligned spins with the anti-aligned spins is what results in the net magnetization, and therefore a higher population splitting is favorable for higher intensity signal.

To effectively deliver the needed radiation to excite the transitions of nuclei, one can think of a vectorial picture where we examine the bulk magnetization as a vector quantity representing the net magnetic moments that are aligned with the external field. This magnetization, $\mathbf{M_0}$ is rotated away from the axis of the field into an orthogonal plane by the application of a second magnetic field, $\mathbf{B_1}$ in a direction we can arbitrarily call the $\hat{x}$ axis. The result of which is more intuitive in the *rotating frame* whereby we observe the magnetic moments of the nuclei in a frame rotating at the Larmor frequency. Effectively, the magnetization in the rotating frame only sees the applied orthogonal magnetic field, when $\mathbf{B_1}$ is applied at the resonance condition, namely that it is rotating at frequency ω, the Larmor frequency in the lab frame. This results in the magnetic moments beginning to precess about the applied field, and the magnetization rotating to align with that field in the rotating frame. The derivation of the resonance condition in the governing differential equations is not reproduced

here, but can be found in entirety in the reference literature, much more elegantly than this author can reproduce [8].

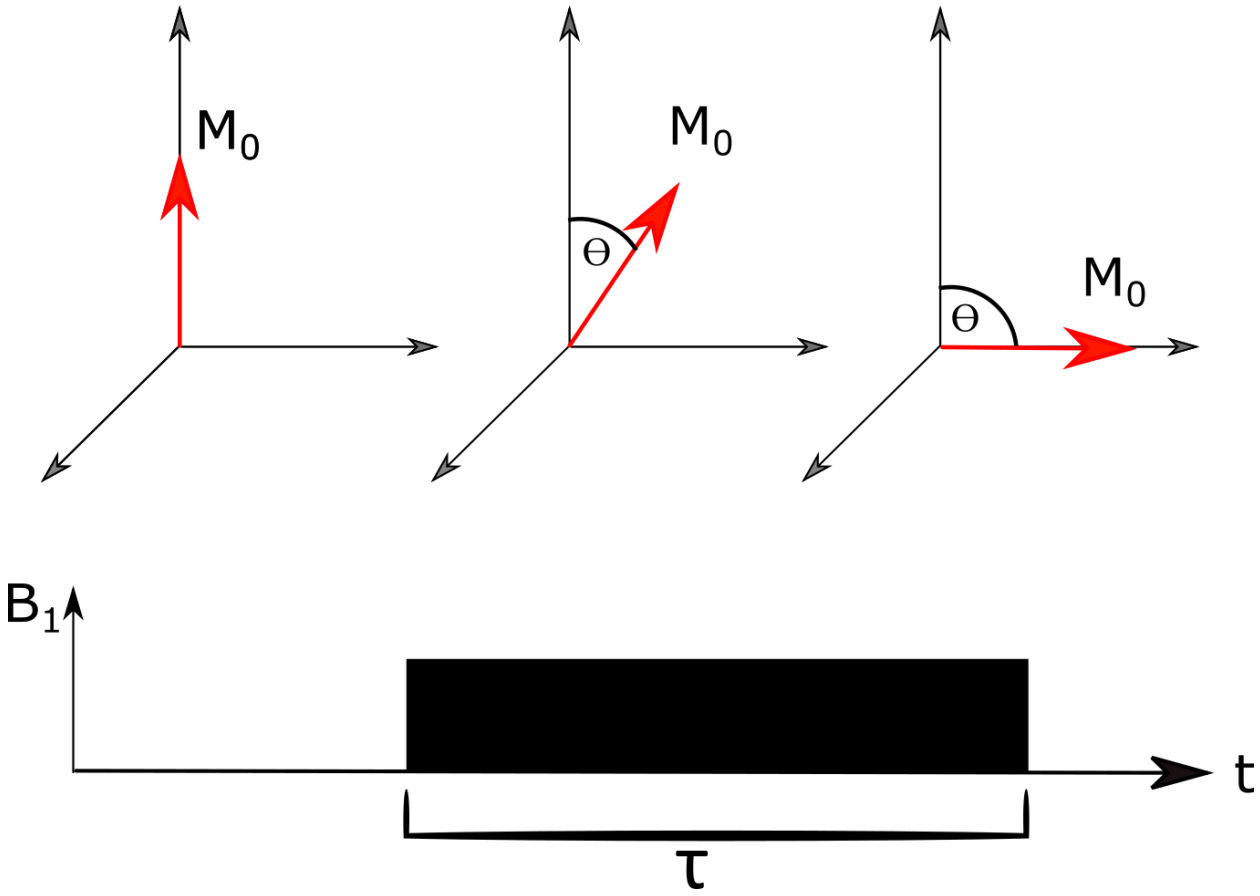

Figure 3. Magnetization evolution with applied orthogonal magnetic field.

What must be clear, however, is that the applied magnetic field $\mathbf{B_1}$ must be rotating at the Larmor frequency in the *stationary* reference frame. In practice, this is achieved by creating a linear-polarized magnetic field pulse in a solenoid type inductor, where the magnetic field oscillates at the desired frequency. The sample is placed in the axis of the solenoid where the magnetic field is most homogenous. A linearly polarized magnetic field may be written as the

sum of two circular polarized magnetic fields, and in the rotating frame, the component that has an opposite rotation to that of the Larmor Precession has negligible effects [8]. Figure 3. details the rotation of the bulk magnetization vector $\mathbf{M_0}$ away from the principal axis, as a function of an applied field. The functional dependence of the tipping angle at the resonance condition of the Larmor frequency are represented by the Bloch equation in three dimensions, giving the precession about $\mathbf{B_1}$ not derived here but once again referred to the reference literature [9]. The result of the Bloch equation when a finite time of applying a constant $\mathbf{B_1}$ is considered gives the tipping angle:

$$\boldsymbol{\theta} = \gamma\tau\mathbf{B_1} = \boldsymbol{\tau\omega_1} \qquad \textbf{[Eq. 9]}$$

where τ is the length in time of the applied pulse and $\boldsymbol{\omega_1}$ the effective frequency of the applied field. A pulse that provides $\boldsymbol{\theta} = \pi/2$ is referred to as a 90° pulse, and effectively places the magnetization into rotation in the transverse plane, orthogonal to $\mathbf{B_0}$.

NMR experiments employ the same coil used to deliver the RF excitation for acquisition [8]. The evolution of the magnetization after being moved away from the static field is governed by the Bloch equations in the lab frame; the solutions of which are reproduced here [9]:

$$\mathbf{M_z} = \mathbf{M_0}\left(\mathbf{1} - \boldsymbol{e}^{-t/T_1}\right) \qquad \textbf{[Eq. 10]}$$

$$\mathbf{M_x} = -\mathbf{M_0}\sin(\boldsymbol{\omega_0 t})\boldsymbol{e}^{-t/T_2} \qquad \textbf{[Eq. 11]}$$

$$\mathbf{M_y} = \mathbf{M_0}\cos(\boldsymbol{\omega_0 t})\boldsymbol{e}^{-t/T_2} \qquad \textbf{[Eq. 12]}$$

These equations introduce several constants, namely T_1 and T_2. T_1 is interchangeably referred to as the spin-lattice characteristic relaxation time, which governs how the magnetization returns to equilibrium with the static field. In subsequent sections the dynamic descriptions of T_1 relaxation

mechanisms will be described. T_2 is similarly and equivalently referred to as spin-spin relaxation time, where the dephasing of the orthogonal components of the magnetization in the x-y plane are understood to be the result of near-neighbor spin coupling. It should be noted that these are the analytic solutions to the Bloch equations in the case of simple relaxation modes, in practice T_2 includes terms due to magnetic dipolar coupling and local magnetic field inhomogeneity (typically referred to as T_2* when including these effects).

In the lab frame, one recognizes from Eq. 11 and Eq. 12 that we have a time varying magnetization in the x-y plane along the two directions. If the coil axis is chosen to be along the $\hat{x}$ direction, then we have a net magnetic field oscillating with frequency $\boldsymbol{\omega_0}$ in the axis of the solenoid. By Faraday's law of induction, we will see an induced current in the coil that can be received over some acquisition time that is scaled with T_2. This induced current will decay in time, due to the exponential decay of spin-spin relaxation effects. The decay of the induced current is known as the Free Induction Decay (FID), as seen in Figure 4. [8]. The induction decay occurs simultaneously to the recovery along the $\hat{z}$ axis in the governing equations, and in most cases $T_2 < T_1$. The resultant FID can be Fourier Transformed (FT) into frequency domain, where the frequency lineshape for a simple 90° pulse is a Lorentzian, centered at the Larmor frequency, with a Full-Width at Half Max FWHM proportionate to $1/T_2$.

While this description phenomenologically describes the experimental acquisition of the induced changes in the spin system, it does not yield descriptions of the interactions governing the relaxation mechanisms present for the bulk magnetization. These analytical descriptions must instead be found in perturbations to the spin Hamiltonian [10].

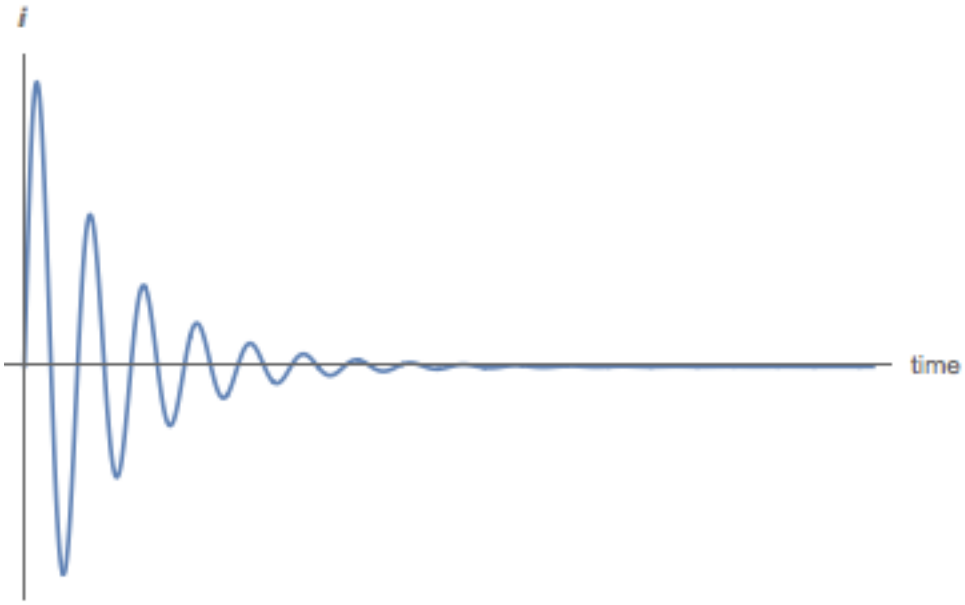

Figure 4. An idealized free induction decay, with arbitrary intensity.

2.3 Brief Comments on Relaxation Formalism

In the introduction of the characteristic relaxation times T_1 and T_2, I have neglected introducing the formalism causing these two decays. The relaxation mechanisms generally arise from several factors in complicated materials. At the moment of the pulse ending in the orthogonal plane, we are left with a magnetization, $\mathbf{M_{xy}}$ that will begin to return to the lower energy configuration, namely by returning to its maximum value with the external field, in the direction of $\hat{z}$. This occurs in the time T_1. At normal temperatures $\frac{kT}{\hbar}$ is very large in comparison to the energies of emitted photons, and so conditions for spontaneous emission of the bulk sample are suppressed. In this case, stimulated emission becomes the dominant relaxation mechanism. The phenomena behind stimulated emission in these bulk systems generally arises from fluctuations in the local magnetic fields and spin interactions within the immediate

environment of the nuclei probed. These mechanisms are dominantly dipolar-dipolar magnetic interactions, but can include higher order interactions as well, such as that of the quadrupole moment with the electric field gradient [10]. In general however, the dipole coupling arises, or is mediated, by the random molecular tumbling in accordance with a Brownian Diffusion process, as well as the intramolecular interactions between neighboring nuclei.

In the formalism of such relaxation mechanisms, the analytic form of the characteristic time over all temperatures and frequencies is generally not determined exactly. This necessitates experiment to probe various dynamics in these complicated systems in order to specify processes and their dominance in a particular material. In liquids, random diffusion behavior accounts for a large portion of the dipolar coupling. In crystalline and amorphous solids, the behavior can be far more complicated. What remains is that by probing the characteristic times T_1 and T_2 we are directly observing the averaging of these interactions over some distribution. The Bloch equations are therefore *phenomenological* in nature. They do not describe analytically the microscopic behavior, but rather a bulk averaged thermodynamic process, which is the resultant sum of quantum mechanical mechanisms. The statistical formalism behind a number of dipole interactions was introduced by Bloembergen, Pound and Purcell in 1948, and in subsequent papers has been derived for a number of specific cases [11]. The derivation of these mathematical descriptions is far beyond the scope of this work, and a full treatment can be found in the appropriate literature, however a note about the dipolar coupling is warranted [10,12].

The interaction between a nuclei and its surrounding magnetic environment was assumed ideal in the Zeeman Hamiltonian expressed above. In general, the Hamiltonian can be re-

expressed as the sum over perturbations to this Hamiltonian, namely:

$$\mathbf{H_0} = \mathbf{H_0} + \sum_i H_i \qquad \textbf{[Eq. 13]}$$

Where the Hamiltonian of two magnetic dipoles interacting through space is given by:

$$\mathbf{H_d} = \mathrm{b}_{ab}[(\mathrm{I}_a \cdot e_{ab})(\mathrm{I}_b \cdot e_{ab}) - \mathrm{I}_a.\mathrm{I}_b] \qquad \textbf{[Eq. 14]}$$

Here b_{ab} represents the dipolar coupling constant, $\mathrm{I}_a, \mathrm{I}_b$ the spin operators for spin A and spin B, respectively, and e_{ab} the unit vector in the direction pointing from spin A to spin B. The note to be made is that the dipolar coupling constant, $\mathrm{b}_{ab} \propto r_{ab}^{-3}$ where r_{ab} is the inter-spin distance. In liquids, this interaction is averaged over many spins and in general is "motionally narrowed" by this averaging [10,12]. Since higher order interactions have increasingly negative power dependence on the inter-spin distance, dipolar coupling is the dominant mechanism. It is further proof that intramolecular dipole interactions are dominant in relaxation phenomena in comparison to intermolecular interactions. In solid systems, more so than liquid, the dipolar interaction can cause broadening of the spectral lines, namely due to the local fluctuations in magnetic fields that are anisotropic relative to the applied field, and so the resultant spectral contribution from each site is distributed. This broadening can be averaged using experimental techniques to reduce these effects.

T_2 behavior can be analyzed in a method analogous to that of T_1 but in general does not encode the same information. T_2 times are more directly related to the broadening of lineshapes through dephasing of the magnetization in the orthogonal plane. Due to this, they are strongly coupled to any inhomogeneity that may be present in the external magnetic field in this plane, as can arise with solenoid type magnets. Furthermore, due to the reliance of the tilting into the

orthogonal plane on the homogeneity of the delivered RF pulse, electronic inaccuracy in the probe itself, either in the orientation of the RF coil relative to the external field, or in power supplied by the external equipment can also result in dephasing that contributes to T_2. The net contributions, including inhomogeneity of the magnetic field intentional or otherwise are therefore encoded in a variable known as T_2^*.

2.4 Chemical Shifts

A particular perturbation to the Zeeman Hamiltonian that is of the utmost importance to NMR spectroscopic techniques, particularly in the fields of analytical chemistry, is known as the chemical shift interaction. This additional element in the Hamiltonian is critical to identifying the chemical structures inherent to large organic and inorganic systems, and allows for the selective probing of particular chemical sites in subsequent dynamic studies. The details will be qualitatively described below, but full treatment of both chemical shift interaction and the closely related Chemical Shift Anisotropy (CSA) can be found in the literature [8,10,12].

In the acquisition of spectrum for nuclei in complex materials, multiple peaks can often be seen at different shifts relative to the central frequency of the spectrum. This arises from the effects of differing electrical environments for the same nuclei at different chemical sites in a molecule. The electrons present in molecules surrounding nuclei also possess spin and magnetic moments, and are actively interacting with the external magnetic field as well. While a formal treatment of the electron interaction with a magnetic field is not given here, it suffices to say that this interaction gives rise to an effective "shift" in the magnetic fields experienced by a particular nuclei in a chemical structure. This "effective" magnetic field can either be additive or opposing

that of the external field, and subsequently affects the frequency of the Larmor precession. As originally stated in Eq. 3, the Larmor frequency is particular sensitive to the magnetic field experienced by a spin. Accounting for the locally affected magnetic field by the presence of electron magnetic moments, we can rewrite Eq. 3 as:

$$\boldsymbol{\omega_{tot} = \gamma \mathbf{B_0} + \gamma \mathbf{B}_{eff} = \gamma \mathbf{B}_{tot} = \omega_0 + \omega_{shift}} \qquad \textbf{[Eq. 15]}$$

Here we have accounted for the magnetic fields produced locally by the electrical environment in $\mathbf{B}_{eff}$, and the resultant frequency as $\boldsymbol{\omega_{shift}}$. In this manner, we can see that the resultant frequency of the signal is no longer centered on the Larmor frequency as predicted by the Zeeman Hamiltonian. The frequency is shifted by a small amount either to a larger or smaller value relative to this frequency. This "shift" can be expressed as the quantity:

$$\boldsymbol{\delta = \frac{\omega_{tot} - \omega_0}{\omega_0}} \qquad \textbf{[Eq. 16]}$$

The chemical shifts for a given electronic arrangement, that is for a known chemical structure or functional group tend to fall within a few Hz of the central frequency or Larmor frequency of the nuclei in question. Because the Larmor frequencies of common nuclei in the magnetic fields of several Tesla are in the radio frequency regime (MHz) these shifts are commonly expressed in parts per million (ppm) relative to the central frequency as given by Eq. 16. The shifts of a particular functional group or chemical species is dependent on factors such as solvents, concentration and ambient temperature, but in general fall within a well-documented range. For referencing purposes, common solvents with very well studied temperature dependent shifts are used in conjunction with the material of interest in order to reference the shifts to a peak of known frequency, as in experiments there is usually some ambiguity in the exact strength

of the magnetic field and Larmor frequencies, as no true isolated spin can be observed. These shifts are tabulated and available both in extensive documentation and online resources.

A further element of note is in the excitation of these peaks relative to the applied pulse. The applied pulse is centralized to a "carrier frequency" of a spectrometer, whereby the central frequency is chosen to be exactly on the frequency of the peak of interest. This is done experimentally, with the frequency usually adjusted by some offset value from the true Larmor frequency of an isolated spin of that nucleus, $\boldsymbol{\omega_0}$, due to its own internal structure. The subsequent peaks that are offset from this frequency, due to their chemical shifts, are therefore not centralized on the spectrum. The pulse being applied is not precisely at an isolated frequency, but in general has a finite width in the frequency domain inversely related to its time scale. Therefore the window of excitation for a given pulse generally covers a wide frequency range, and will excite shifted peaks. Typically in experiment, we do not worry if these peaks are properly centered, as the *evolution* of their amplitude with other quantities in a pulse sequence, as discussed below, are more revealing.

Chapter 3: Experimental Details and Pulse Sequences

3.1 Inversion Recovery

In order to measure dynamic quantities in NMR such as T_2 and T_1 or more difficult quantities such as ionic diffusion coefficients (D), a number of different pulse sequences can be employed to extract the relevant time evolution of an NMR signal with respect to that dynamic quantity. In the case of a measurement to find characteristic time T_1 one can employ what is

known as an Inversion Recovery sequence, whereby the magnetization $\mathbf{M_0}$ is rotated 180° to oppose its original orientation along the $\hat{z}$ axis. A period of time denoted by τ is then allowed to pass before a second pulse that rotates the magnetization by 90° is applied, which then aligns the magnetization along the acquisition axis. An intensity measurement (either of the resultant initial voltage of the FID or an integral of the spectra) can then be taken, as a function of the time allowed between pulses. This recovery curve can be described analytically by the expression:

$$\mathbf{M} = \mathbf{M_0}(\mathbf{1} - \mathbf{2}e^{-\tau/T_1}) \qquad \textbf{[Eq. 17]}$$

the plot of which can be seen in Fig. 5, along with a schematic of the pulse sequence.

In practice, an inversion recovery curve is obtained with discrete values of tau arrayed at values along the curve that are dependent on the nuclei and material in question. Furthermore, different chemical sites can be isolated if the spectral peaks are distinguishable, and their individual recoveries can be obtained in a similar manner. This allows for the extraction of T_1 dynamics available to particular chemical structures.

There are cases where an inversion recovery sequence is not ideal for the extraction of T_1. These cases are where T_1 is particularly long, or a peak requires long pulse widths and power to achieve inversion. In these cases, the time scales of the total experiment will be very long, or in some cases the limit of available power will lead to longer pulses that can introduce unwanted dephasing or echo formation in the acquired signal. A method to combat these effects is to use a saturation recovery sequence, the details of which can be found in the literature [10,8]. An analogous technique can be used to extract T_2 values, but is beyond the scope of this work.

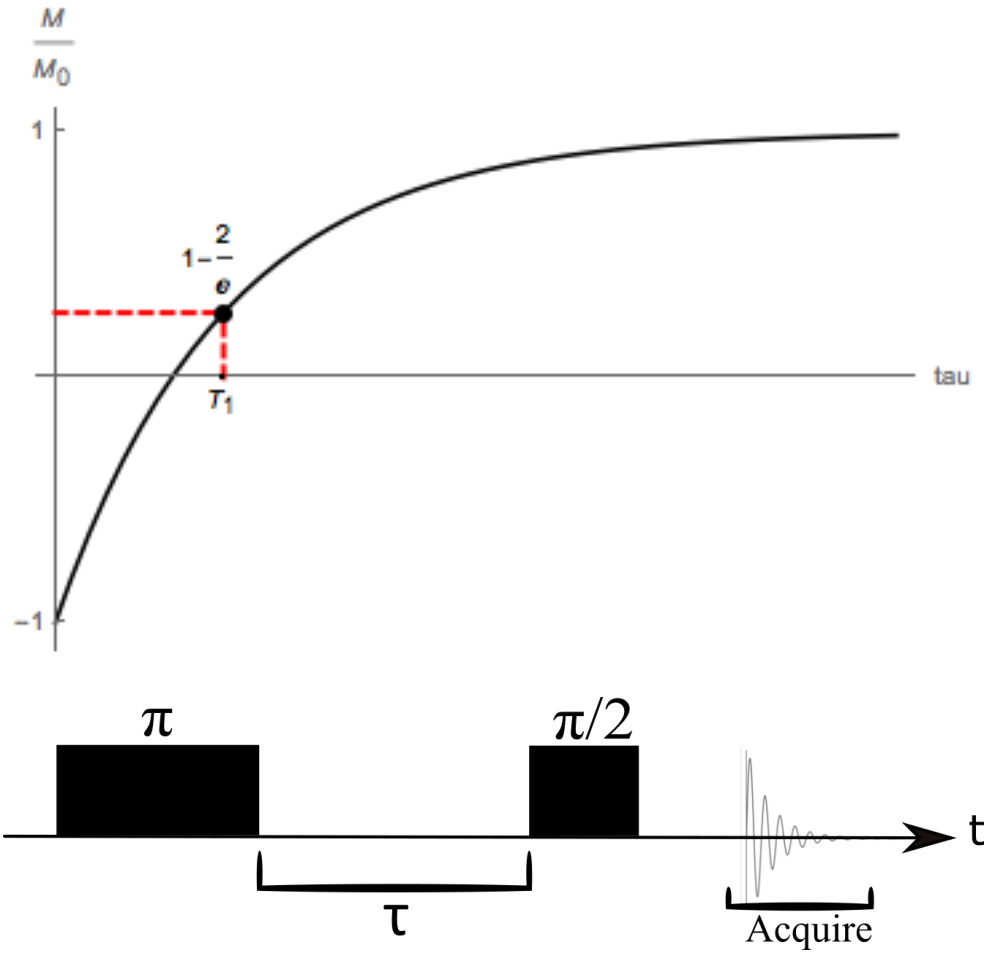

Figure 5. A T_1 Inversion Recovery, with accompanying schematic pulse sequence.

3.2 Static Gradient Diffusometry

In electrochemical materials, we are particularly interested in the transport of charge in bulk systems. This mechanism is critical for materials that act as electrolytes in batteries, where the ion that is formed as a result of the redox reaction is moved in a material that is not electrically conductive, so that the work is done on the external circuit. It becomes necessary, in order to examine candidate materials, to look at the effective diffusion of these ions, and lithium ions are only one scenario where this is desired. Diffusion here refers to *Brownian Diffusion*

whereby assumptions that the system is experiencing no driving external forces, and no major chemical potential gradient. This diffusion is random in nature, and is driven purely by thermodynamic principles.

This can effectively be measured by NMR techniques. Through the Nernst-Einstein equation given by Eq. 18 one can directly relate the self-diffusion coefficients to the ionic conductivity of a material.

$$\boldsymbol{\sigma} = \frac{F^2[C]}{RT}(\boldsymbol{D}_+ + \boldsymbol{D}_-) \qquad \textbf{[Eq. 18]}$$

Here $\boldsymbol{\sigma}$ is the ionic conductivity, F is given by Faraday's Constant, R the gas constant, T the temperature and [C] a parameter that relates the valences of the ions and the number of ions per chemical unit. $\mathbf{D}_{\pm}$ are the self-diffusion coefficients of the cation and anion, respectively.

From the measurement of the diffusion coefficient, one can further extract average molecular size via the Stokes-Einstein equation:

$$\mathbf{D}_{\pm} = \frac{kT}{6\pi\eta r} \qquad \textbf{[Eq. 19]}$$

Here k is Boltzmann's constant, η is the dynamic viscosity of the liquid, and r the average radius. This expression encodes assumptions that the particles can be treated as spherical like, moving in a fluid dominated by laminar flow. Other dynamic fluid models can be used to relate diffusion coefficients to molecular information as well.

To extract the diffusion coefficient experimentally, NMR experiments known as Pulsed Field Gradient (PFG) techniques are typically used [8,10]. These techniques employ a probe that is cable of supplying a secondary magnetic field that is coaxial with the external magnetic field, but varies spatially along the axis. This is referred to as the magnetic field gradient, and it was

shown by Stejskal and Tanner in 1965 that with a spin-echo sequence (further details given below) and this gradient coil, one could encode the positions of nuclei in the material as a function of their positions relative to the gradient [13]. The resultant expression for the decay of the magnetization in the presence of a gradient field is given by:

$$\mathbf{M(t) = M_0} e^{[-\frac{2t}{T_2} - D\delta^2 g^2 \gamma^2 (\Delta - 1/3)]} \qquad \textbf{[Eq. 20]}$$

In this expression, δ is the length of the applied gradient pulse, *g* the gradient strength, γ the nuclear gyromagnetic ratio, Δ the diffusion time allowed between gradient pulses. In this form, the equation is measured using a spin-echo sequence in which the following occurs. The magnetization is rotated into the orthogonal plane via a 90° pulse, and then a spatial gradient is applied for some time δ. During this time the signal undergoes dephasing in the plane due to T_2 effects. The gradient has the effect of changing the magnetic field at each point along the gradient axis, and therefore changing the frequency of the nuclei at each position. After some time, known as the diffusion time Δ, a 180° pulse is applied which rotates the now dephased spins in the orthogonal plane into the opposite half. These spins begin to rephase in the plane, when a spatial gradient in the opposite direction but of the same strength and duration are applied, the effect of which is to cancel out the effects of the first gradient. If this is successful, the original frequency offset of the first spatial gradient would be cancelled and the signal would just be returned as in a normal experiment. If the ions have undergone their Brownian Diffusion however, the offset will not be corrected as they have moved from their original positions and therefore the secondary gradient is not acting on the same nuclei in the same position. The result of this is an overall signal attenuation that is proportionate to one of two factors- the diffusion

time, or the strength of the magnetic gradient. It should be mentioned this displacement is Root Mean Square (RMS) displacement, not absolute, as it is only an averaged displacement relative to the gradient axis.

In PFG experiments the magnetic field gradient strength is changed, and the resultant attenuation of the magnetization as a function of this parameter is acquired. The overall curve follows a Gaussian type shape, and is only affected by T_2 attenuation in the plane on the time scales of the entire pulse sequence. Due to limiting experimental effects such as the restrictions on gradient strength due to power requirements, small diffusion coefficients can be difficult to measure (small relative motion along the gradient axis). PFG probes also suffer from Eddy currents induced by the flux of magnetic fields in the surrounding probe housing, that can be received during signal acquisition and interfere with the signal of the sample. There are experimental techniques to combat these effects with various delays during the pulse sequence.

An alternative technique, which shall be focused on in this work, is the measurement of diffusion coefficients in a static magnetic field gradient, using the same formalism outlined briefly above, but with a variation of the parameter known as the diffusion time instead of the gradient strength. In the case of a constant magnetic field gradient with varying time for diffusion, the expression derived by Stejskal and Tanner is rewritten as:

$$\mathbf{M}(\boldsymbol{\tau}) = \mathbf{M_0} e^{-\frac{2\tau}{T_2} - Dg^2\gamma^2\tau^3} \qquad \textbf{[Eq. 21]}$$

where now we consider a fixed field gradient strength and include the time allowed for diffusion in the variable τ. Note that the dependence on $\boldsymbol{\tau^3}$ now involved arises from the considerations of the dephasing of a magnetization as the time of exposure to a gradient limits to infinite.

In practice, we now have to consider the attenuation of signal due to T_2 effects in addition to that caused by gradient. To achieve a static magnetic field gradient, the sample can be placed in the non-homogenous field below the central axis of a solenoid magnet, which has a permanent gradient that runs along the central axis. These gradients are generally a factor of ~10 larger than those produced by PFG gradient coils, for example in an 11T magnet, the peak gradient value was found to be 5.5kG/cm. This means that the second term in the exponential is dominant (this is scaled with the square of the gradient strength) and therefore with large gradients T_2 attenuation is sub leading. In order to acquire the magnetization intensity as a function of the diffusion time, the same pulse sequence mentioned above is employed, detailed in Fig. 6. and the same encoding-decoding mechanism is achieved. Magnetic field strength is calculated as a function of position using a gaussmeter (Lakeshore company), with measurements taken in cm increments. The gradient value is calibrated by using a sample of known diffusion coefficient, such as protons in water, and a reverse analysis is done to extract gradient strength. Attenuation is recorded as a function of discrete values of τ, which are arrayed depending on the observed amount of diffusion present in the sample. The only major difference is the absence of the gradient pulses in the sequence, and acquisition begins immediately after the second pulse.

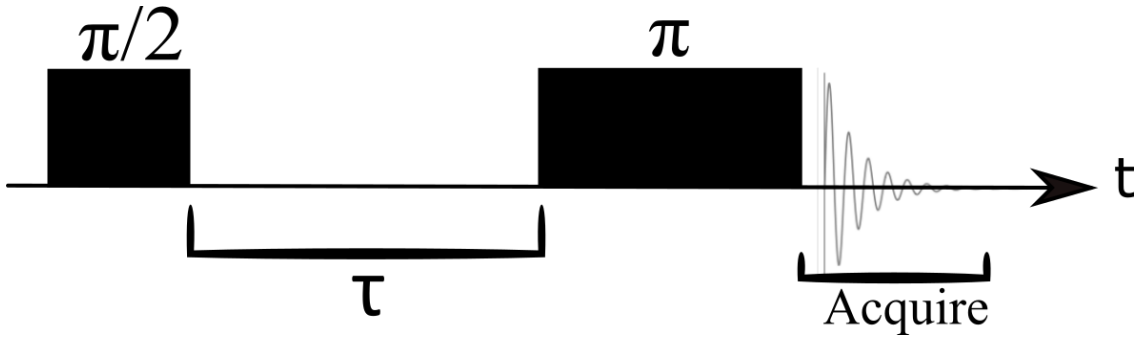

Figure 6. Spin echo pulse sequence used in diffusion measurements.

3.3 High Pressure NMR

Thermodynamic variables are important in the full mechanistic understanding of a complex system. Temperature, pressure and volume are critical quantities in understanding the behavior of materials in various environments, and make up the equation of state for any given system. From a thermodynamic formal standpoint, there are multiple variables that may be advantageous to view a particular system in, such as entropy or the notion of free energy, but intuitively these are not quantities we can associate with the majority of physical phenomena in our daily lives. From an experimental standpoint, there are a number of ways to efficiently change temperature in a sample, however this gives us only one degree of freedom to explore the thermodynamic properties of a system. Often, by increasing temperature in a closed system we also increase volume by expansivity, but also increase the average kinetic energy available to the constituents of the system. In providing this increased average energy, the dominance of certain statistically weighted processes becomes skewed- a key example is molecular diffusion, which greatly becomes more involved in dipole relaxation at higher temperatures due to increased molecular tumbling relative to their magnetic environment.

It is advantageous to study materials using multiple thermodynamic variables, and variable pressure studies provide a unique insight into volumetric dependencies without changing internal energies. Whereas the increase in volume due to thermal expansion is accompanied by an increase in average kinetic energy, the increase of pressure decouples the change in volume from the change in internal energy. This allows the probing of processes that are specifically dependent on things such as a decrease in the free volume available to a molecule

or functional group. The key dynamic quantity that can be studied in variable pressure NMR techniques is the activation volume:

$$\mathbf{\Delta V = -kT\left(\frac{\partial \ln \alpha}{\partial P}\right)_T} \qquad \textbf{[Eq. 22]}$$

where ΔV is the activation volume, in units of inverse volume, T is the temperature, P is the pressure, and α is the dynamic variable of interest. In NMR studies it is commonly the inverse of T_1, known as the relaxation rate $R_1 = \frac{1}{T_1}$, or the self-diffusion coefficient, D. This quantity expresses the dependence of a molecular process on the available free volume, and so is representative of the minimum free volume necessary for this process to occur in an analogous form to an activation energy, which describes the minimum energy necessary for a process.

To realize high pressure conditions in an NMR experiment, specialized equipment in the form of a probe designed to withstand hydraulic pressures while still performing the necessary electrical properties is needed. This probe is similar in construction of the electronics to other standard NMR probes, but possesses a specialized sample-housing chamber made of a copper-beryllium alloy. This alloy is robust enough to withstand high pressures in a small volume that encapsulates the acquisition coil, the center of which is where samples are placed during experiment. The coil leads are then passed through a "plug" (that is impermeable to liquid) and allowed to reach the lower area of the probe where the RF circuitry is placed. This housing is then filled with hydraulic fluid via a small nozzle opening at the other end of the chamber. Pressure is typically applied using a perflourinated hydrocarbon liquid (Flourinert, 3M Company), which is pumped into the chamber with the use of a single-piston lever action hydraulic pump commercially available (Enerpac Company, an Actuant division) in ranges of [0-

250] MPa. This liquid is adequate for all nuclei except for studies that wish to probe fluorine nuclei, in which case an equivalent viscosity conventional hydrocarbon can be substituted. Flourinert offers the key advantage of being chemically inert, and possesses a high thermal conductivity allowing for efficient cooling of the interior of the probe [14].

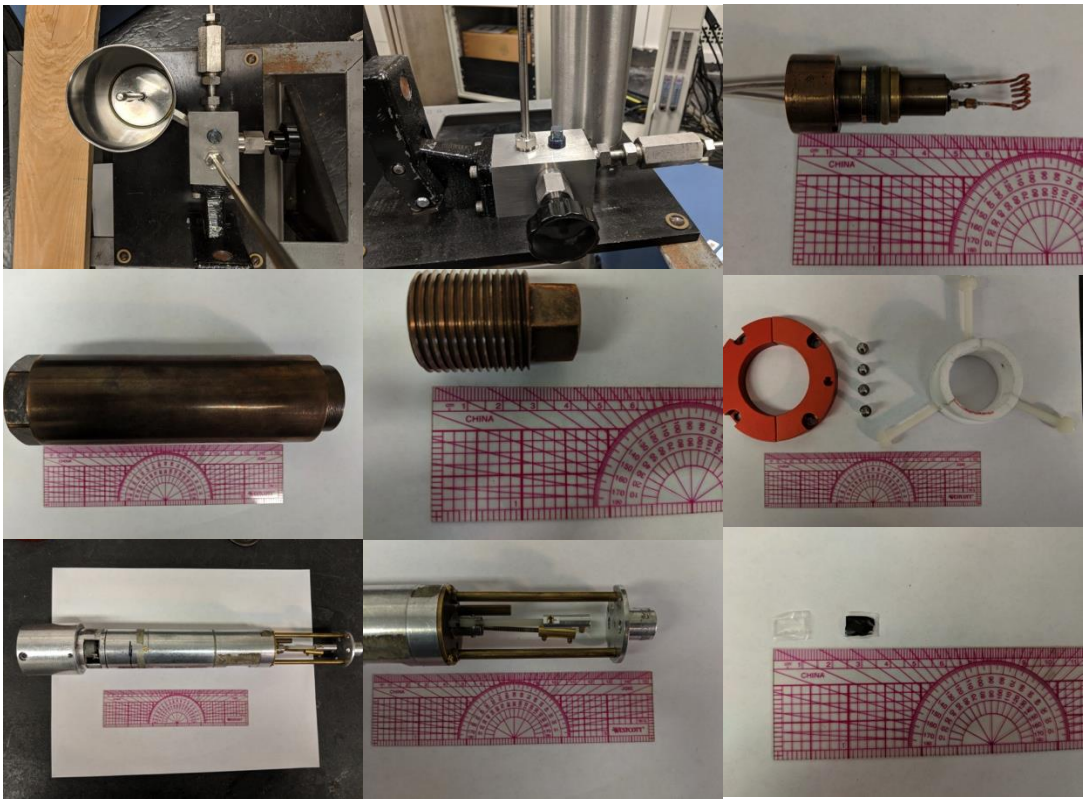

Figure 7. From left to right: Flourinert reservoir, Hydaraulic pump assembly and plumbing, High pressure "plug" with diffusion coil, High pressure probe chamber, Chamber sealing nut with through-hole for coil leads, Mounting hardware to secure to magnet bore, Lower probe section containing RF wiring, Probe tuning capacitors, Examples of high pressure samples packed in polyethylene bags.

To pack samples in the coil without exposure to liquid contact, materials are packed hermetically in polyethylene bags of sub-mm thickness. The bags are sealed using an impulse sealer at low temperatures. Polyethylene films are amorphous at ambient temperatures and a wide range of pressures, and so effectively transmit pressure to the material of interest without

interference [15]. The high pressure chamber, being a copper alloy, is conductive electrically. This makes it subject to the induction of high Eddy currents in the present of strong time-dependent magnetic flux, and so conventional PFG techniques for measuring diffusion are impossible. To account for possible induced currents during normal pulse sequences, an acquisition delay is present after the final pulse to allow time for the decay of these localized currents.

Several images representative of the high pressure probe and hydraulic assembly are given in Fig. 7. to provide a physical reference. All other facets of conventional NMR experiments, as detailed above, remain entirely valid for high pressure experiments. In the work discussed in subsequent sections, the dynamic quantity measured will be outlined in the discussion of that particular material system.

3.4 Fast Field Cycling NMR

Another variation of conventional NMR experiments that has only been realized in experiment relatively recently is that of Fast Field Cycling (FFC) NMR. The frequency dependence of relaxation phenomena is understood through BPP formalism as described in discussion of relaxation phenomena in the previous section. Many interactions are detailed in analytical form in the relevant literature as well, but widespread experimental support for NMR spectrometers capable of varying frequency only became available in the early 2000's [16-18].

This technique functions in an analogous manner to a simple one-pulse experiment at a static magnetic field, however in FFC experiments the strength of the magnetic field can be changed from very low fields to a maximum just below 1T in commercially

available instruments (Stellar Company, Italy). For ^{1}H NMR, this corresponds to a maximum frequency around 40MHz. In order to provide the variable magnetic field strengths, a solenoid type electromagnet powered by a 400A three-phase power supply is used, with a finely tuned power supply control unit that can reproduce magnetic fields with precision. The magnet sits in a Flourinert bath, which is subsequently cooled via a water-based heat exchanger pump. Variable Temperature (VT) measurements are also commercially supported, with low temperatures achieved with a liquid nitrogen evaporator and high temperatures via an internal air-heating element. Samples in FFC measurements are packed in borosilicate 5mm radius NMR tubes. The majority of FFC measurements focus on T_1, but experiments to measure T_2 values are also available and supported in commercial units [16].

The experimental design can be described by now considering the strength of the *external* field as a function of time. In this case, the Larmor frequency as derived in Eq. 3 will vary with the strength of this field, during the course of the experiment. Initially, no magnetic field is experienced by the sample. At time t=0, a magnetic field referred to as the "relaxation" field is applied in the laboratory $\hat{\boldsymbol{z}}$ axis, resulting in a net magnetization growing along this direction, exponentially related to T_1. After time τ has elapsed at this magnetic field strength, the external field is increased linearly to what is known as the "acquisition" or "detection" field. The purpose of this magnetic field is to be able to excite the nuclei with RF at a frequency within the optimal range for the probe. A 90° pulse is applied, and the amplitude of the magnetization resulting from this pulse in the orthogonal plane is measured instantaneously. The magnetic field is then switched off and the spins allowed to entropically equilibrate, after which the sequence is

repeated for a smaller value of τ resulting in a smaller amplitude of the magnetization, according to same recovery expression given in Eq. 10. This can of course be done from short τ to long τ depending on sample signal strength and the time of T_1. After T_1 is obtained for a given relaxation field strength, this sequence is repeated for a different value of the relaxation field, and therefore a different frequency. A schematic diagram of the magnetic field sequence during a single sequence can be found in Fig. 8.

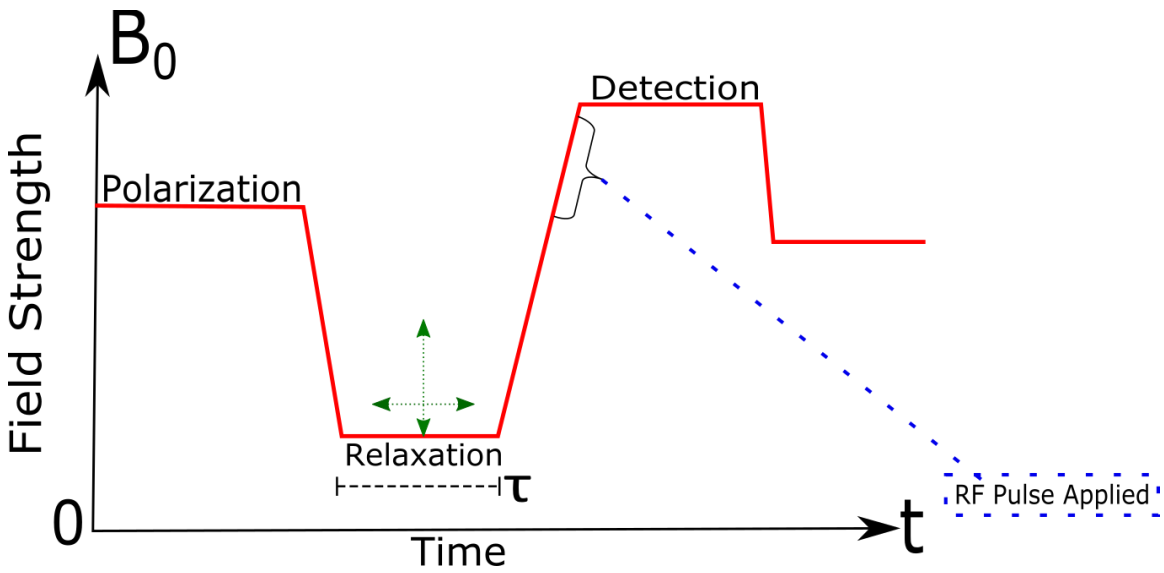

Figure 8. Schematic of magnetic fields during FFC experiment.

The number of fields swept can be chosen to best characterize dynamics in a specific system, and the entire process is software controlled via commercial units. Some limitations on the magnetic fields chosen arise due to the concentration of the chosen nuclei in the sample, as those with lower concentrations suffer from low Signal-to-Noise (S/N) at low magnetic fields due to noise from various ambient sources. This can be addressed using a pre-polarizing sequence, which applies a magnetic field for a fixed amount of time prior to the relaxation field. This has the effect of building up initial magnetization strength, to help distinguish signal from

noise, and is kept constant for all values of τ in the sequence. Furthermore, values of T_1 can be very short in fast-relaxing systems, such as solids at low temperatures, and can approach the switching time (sw) involved in increasing the magnetic field from the relaxation field to the acquisition field. In typical experiments sw ~2ms and so T_1 values that approach this limit cannot be considered.

In FFC measurements, the relaxation profile given by the inverse of T_1 (R_1) as a function of frequency is acquired, and subsequently needs to be interpreted from a first-principals standpoint. As discussed in prior sections, T_1 is dominated by dipolar interactions, which can be mediated through molecular dynamics that can be site specific in complex molecules. FFC allows for the frequency dependence of these interactions to be explored [16-18]. At varying temperature, certain interactions can be isolated as the principal component of the relaxation. One example is that of the low frequency, high temperature limit of the relaxation curves, which can almost entirely be attributed to molecular diffusion processes, and subsequently analyzed using a simple linear expression given by:

$$\mathbf{R_1}(\boldsymbol{\omega}) = \mathbf{R_1}(\mathbf{0}) - \boldsymbol{N_i}\left(\frac{\boldsymbol{\mu_0}}{\mathbf{4\pi}}\boldsymbol{\gamma_i^2}\hbar\right)^{\mathbf{2}}\left(\frac{\sqrt{\mathbf{2}}+\mathbf{8}}{\mathbf{30}}\right)\left(\frac{\boldsymbol{\pi}}{\boldsymbol{D}}\right)^{3/2}\sqrt{\boldsymbol{\omega}} \qquad \textbf{[Eq. 23]}$$

which was analytically derived for relatively low viscosity ionic liquids by D. Kruk et al. [19]. Here R_1 is a function of the applied magnetic field (frequency), $\boldsymbol{N_i}$ is the number density of the nuclei denoted by index (i), $\boldsymbol{\mu_0}$ the vacuum permeability, $\boldsymbol{\gamma}$ the gyromagnetic ratio of the nuclei studied, $\hbar$ the reduced Planck constant and **D** the self-diffusion coefficient. Through this approach in the extreme limit of frequency, relaxation curves can in fact be used to derive self-diffusion coefficients for species, with some initial knowledge of the chemical nature of the

moving species.

The formalism behind the analysis of resultant relaxation profiles require careful discrimination between the interactions present in a system, and are generally in need of support from parameters acquired by other experimental means. These parameters may be the average interatomic distance between neighboring chemical sites or the viscosity of a bulk sample [16]. A number of higher order interactions can be accounted for in relaxometry, making it a robust technique for characterizing dynamics in complicated systems.

Chapter 4: Fast Field Cycling Studies of BMIM TFSA

This work has been accepted in the Journal of The Electrochemical Society and was done in collaboration with Dr. Sophia Suarez of Brooklyn College, CUNY, Dr. James Wishart and Dr. Jasmine Hatcher of Brookhaven National Laboratory. First author on this work was Dr. Kartik Pilar, and the author of this thesis was a co-author, contributing to the section on FFC Studies in collaboration with Dr. Shen Lai.

4.1 Introduction and Sample Preparation

Ionic Liquids (ILs) are systems of salts that are liquid at room temperatures, which have found application in a variety of fields, not least of which as non-volatile electrolyte solvents in lithium ion batteries [20,21]. They are desirable for a number of reasons, including: low vapor pressure, selective properties in the form of cation and anion structures, and thermal stability [22]. These properties make them good candidates for electrochemical systems, but need to be further understood on a molecular level in order to enhance performance. IL's generally have

high viscosities, and consequentially low ionic conductivity values. In order to combat these drawbacks, investigations of the dynamics in IL systems reveal the effects of altering salt chemical structures. A full relevant discussion of the effects of altered chemistries can be seen in the well-established body of literature [22]. In attempts to understand the complicated dynamics of IL systems, techniques such as molecular dynamics simulations and Raman spectroscopy have been employed [23-25]. In this study, NMR characterization, specifically high pressure multinuclear studies, are presented to further elucidate molecular dynamics in the 1-butyl-3-methylimidazolium bis(trifluoromethylsulfonyl)amide (BMIM TFSA) species of IL, and several isotopologues. For the purpose of this thesis, this work will briefly outline the FFC studies done on the pure BMIM TFSA chemistry and its use in comparison to conventional PFG techniques.

Sample preparation was done at Brookhaven national laboratory, the details of which can be found entirely in the supplementary materials of the resulting publication [22]. For the purposes of FFC studies, BMIM TFSA IL was stored in an argon-filled glovebox to avoid ambient moisture contamination. After drying in a vacuum oven at low heat over approximately one day, samples were packed in the glovebox into 5mm FFC NMR tubes and sealed with Parafilm (Bemis Company).

4.2 Experimental Details and Results

FFC measurements of ^{1}H spin-lattice relaxation times T_1 were carried out at frequencies ranging from 100kHz to 35MHz in 15 logarithmically spaced increments. These measurements correspond to the ^{1}H sites on the BMIM cation in the salt. These T_1 curves were collected in a temperature range of 263-333 K in increments of 5K. For frequencies below the threshold of

12MHz, a pre-polarizing magnetic field sequence was used, as detailed in a prior section, in order to combat low S/N. As detailed in the previous section on FFC experiments, relaxation phenomena for T_1 primarily arise from dipolar interactions that are both intramolecular and intermolecular in nature [10,12]. Intramolecular interactions are typically much faster reorientation processes that involve bond angle fluctutations and conformal exchange of the molecule leading to local magnetic field interactions. Intermolecular interactions generally evolve from the molecular tumbling through a surrounding magnetic environment.

The relaxation curves can be described via spectral density functions, which arise from the Fourier Transform (FT) of the autocorrelation functions that describe specific molecular processes. The time scale of these processes is proportionate to the correlation time, which can be found via T_1 minimum as a function of frequency. In general, the correlation time associated with intermolecular processes tends to be shorter than that associated with intermolecular processes [10]. Fig. 9 shows ^{1}H relaxation rates R_1 as a function of Larmor frequency, ω. The qualitative trend is a decrease in R_1 with increasing frequency, corresponding to an increase in T_1. This can by intuitively understood as a reflection of the increased equilibrium conditions of the bulk sample with the external field. At higher magnetic fields, the local magnetic environment of the system is increasingly coupled or well ordered relative to the external field, making local fluctuations in magnetic environments less powerful as a relaxation pathway for the magnetization. We also see a general decrease in R_1 with temperature, which is a reflection of the higher average kinetic energy available to the bulk system. As temperature increases, diffusion becomes the dominant interaction in dipolar coupling. As a result, the local magnetic fields are

averaged out by the nature of this stochastic process, increasing time that relaxation takes to occur.

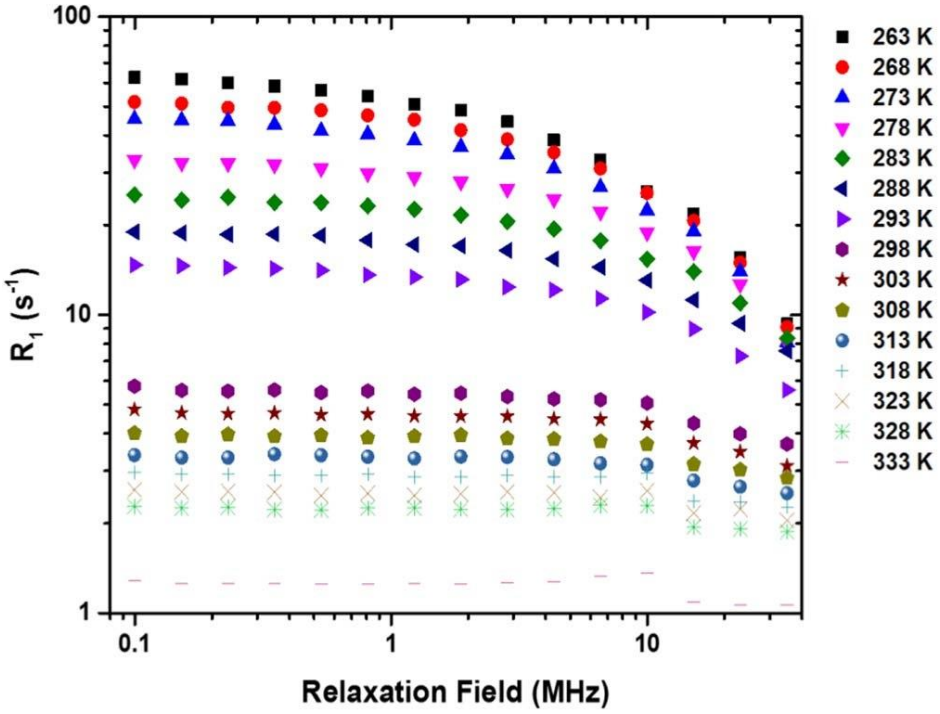

Figure 9. ^{1}H Relaxation rates R_1 at selected Larmor frequencies for BMIM TFSA.

In the low frequency and high temperature limit the diffusion coefficient for molecule with the probed nuclei can be represented by Eq. 23, and is here used to extract **D** values of the ^{1}H carrying BMIM cation. The low frequency upper limit was taken to be 1.5MHz for all temperatures, despite higher temperatures remaining linear over the entire frequency range. The results of this calculation are presented here in Fig. 10. A general increase in the value of **D** with temperature is demonstrated, as expected classically. Good agreement is found with **D** values for $BMIM^+$ measured using PFG techniques, supporting the argument that this low frequency limit can be used to extract self-diffusion coefficients. Eq. 23 is presented with some

simplifications of the spectral density functions at low magnetic field strengths, namely that the faster reorientational processes also represented in the spectral density functions are sub-leading in the expression for relaxation in this limit. This is qualitatively supported by notion that low frequency values are coordinated with processes with longer average correlation times, such as translational motion. The expression also attributes all translational dipolar coupling to homonuclear interactions only- that is only the ^{1}H near neighbor interaction is being considered [19]. This is a valid assumption considering protons dominate the number density in the expression, $N_{H,}$ and is demonstrated by the agreement show in Fig. 10.

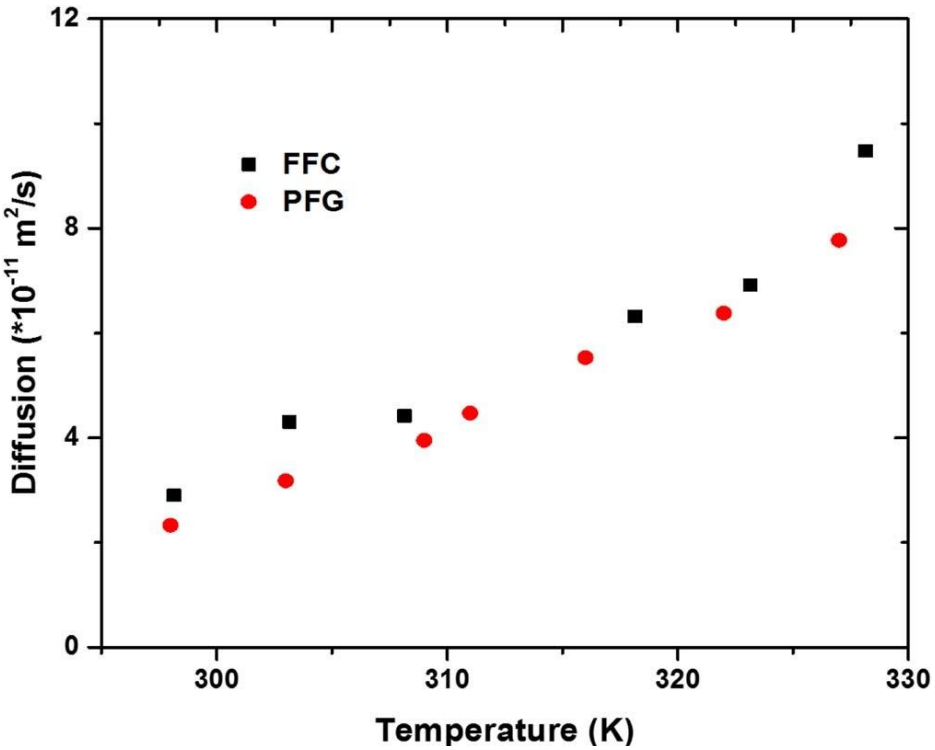

Figure 10. ^{1}H Self-diffusion coefficients calculated as a function of temperature from FFC with those found via PFG.

4.3 Conclusions

BMIM TFSA isotopologues have been characterized via HP NMR and FFC NMR

techniques. For the purposes of this thesis, FFC studies were focused on, and their analysis with respect to simplifications of the BPP formalism behind relaxation phenomena. This analysis demonstrated the validity of assumptions taken in the dominance of homonuclear dipolar coupling in comparison to the heteronuclear coupling, and the assignment of the low frequency limit to translational behavior. This analysis is supported by the agreement of PFG and FFC diffusion results for the $BMIM^+$ cation. Table 1, containing R_1 data measured via FFC at varying temperature, is available in appendix A. Further details of the HP studies and NMR characterization of IL dynamics can be found in the published article [22].

Chapter 5: High pressure Diffusometry of Novel Polymer Electrolyte

This work was done in collaboration with Ionic Material Company, Woburn, Massachusetts on a novel material of proprietary nature. The HP diffusion studies presented here are unpublished as of the time of writing this thesis, and were done by this author at Hunter College. Additional NMR material will subsequently be found in a publication in the near future.

5.1 Introduction and Sample Preparation

As discussed in the introductory section on battery chemistries, specifically those of rechargeable secondary batteries, the common problem with commercially available lithium ion batteries lays within the flammable electrolyte solvent material. Solid state alternatives to electrolyte materials have been a prominent area of research for decades, both in ceramic and amorphous polymer type materials. Although advances in this research have been great over the past few decades, performance of these solid-state alternatives remains subpar for widespread application [3,4]. Ceramic based electrolyte materials suffer from low conductivity at room

temperature, as well as limited specific capacity [3]. Furthermore, they have shown to not be impervious to dendrite formation problems as previously believed on a large scale [4]. Polymer electrolytes are an area of great interest for their many beneficial characteristics. Amorphous polymers are solids at a wide range of temperatures and can be tailored in chemical structures along the polymer backbone and polar end groups, as well as flexibility in molecular weight. Solid polymers are structurally ideal electrolytes as they can both solvate the polar lithium salts and also act as the porous separator, increasing energy density in a cell. Since the mid-90's, Poly(Ethylene)-Oxide based polymer electrolytes have been the focus of much research, mainly for its robust mechanical properties and widespread availability. PEO based systems have however remained relatively unviable commercial because of their low conductivity at ambient conditions (less than 0.1 mS/cm) [26].

Ionic Materials Inc. (IM) has recently developed a novel solid polymer electrolyte material that shows profoundly impressive electrochemical properties at ambient conditions, and this thesis presents here a part of a larger body of work intended to characterize and understand this material. In this work a brief discussion of HP-NMR ion self-diffusion coefficients for the IM polymer is presented.

The IM polymer electrolyte material was supplied by Ionic Materials, Woburn, Massachusetts and stored in an argon glovebox to avoid moisture contamination. IM resident researchers fabricated all materials relevant to this discussion. The samples contain, in varying concentrations, lithium salts. The lithium salt responsible for the ^{7}Li ions studied in this work is Lithium bis(trifluoromethanesulfonyl)imide (TFSI). Due to the highly proprietary nature of this

material, full details of synthesis and material composition will not be presented here.

Conventional PEO based polymer electrolytes are believed to transfer lithium ions within the polymer matrix via a "charge hopping" mechanism. This mechanism is believed to be a movement of the ions along the ether oxygen groups present along PEO backbones [26]. Such a motion is heavily dependent on the segmental fluctuations in the polymer, as the ether oxygens need to be in the proper configuration for the hopping to occur. This mechanism, has demonstrated in a wide range of PEO samples to be inefficient at conducting ions, and at higher pressures is likely heavily suppressed. The novel IM polymer material is believed to function in a method independent of the polymer segmental motion, via a charge-hopping mechanism that utilizes charge defect sites along the polymer backbones, which is decoupled from the polymer segmental motion. Ionic diffusion measurements at room temperature indicate that this mechanism is far more robust and efficient that the hopping in PEO based systems, and is groundbreaking in performance for polymer electrolytes [26]. HP-NMR studies are intended to demonstrate this decoupling.

5.2 Experimental Details and Results

IM Polymer material was packed into polyethylene HP-NMR sample bags, and impulse sealed under low heat in an argon glovebox to avoid ambient moisture content. Samples were rectangular and as thin as experimentally possible; roughly 10mm by 6mm square and 1mm thickness. These bags were then placed in a "flat" induction coil of the HP-NMR probe, to allow for only a thin cross section to be exposed to a field gradient. After assembly, the probe was placed in the lower part of an 11T (Oxford company) (500MHz) superconducting magnet with a

Varian spectrometer. The position was measured using a gaussmeter as detailed in the experimental section above, and a screw-type jack is used to raise or lower the probe position in sub-mm increments. Position and gradient strength were calibrated using a reference sample of lithium chloride (LiCl) in water. Diffusion of ^{7}Li in this reference was measured using PFG in a 7T (300MHz) magnet and Varian Spectrometer, using a DOTY z-gradient diffusion probe. Calibrated gradient value is 5.94kG/cm at the position used (coil height was approximately 17cm relative to the bottom of the magnet).

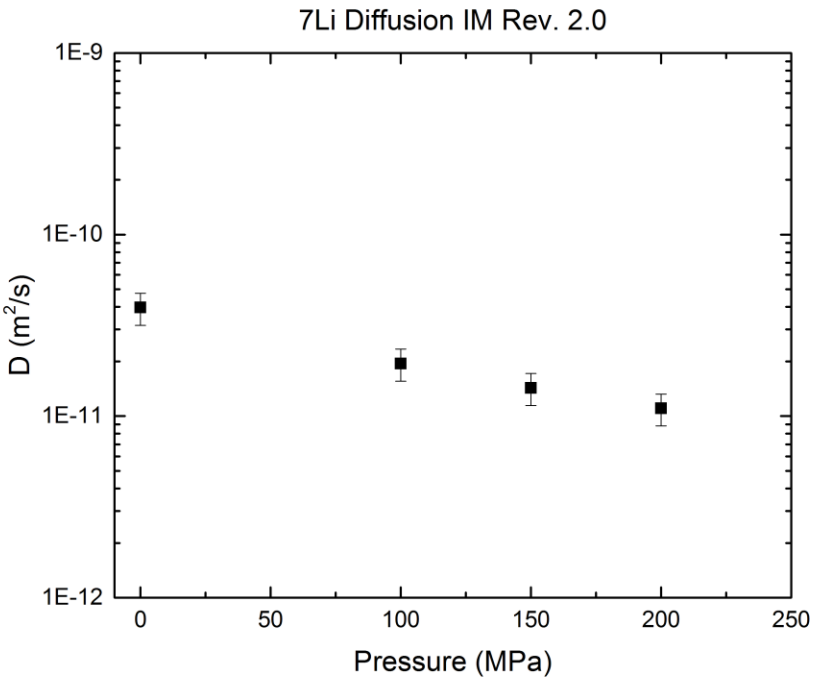

Figure 11. ^{7}Li D values for IM Rev 2.0 as a function of applied pressure.

A spin echo pulse sequence as detailed in Fig. 6 was employed to measure ^{7}Li self-diffusion coefficients. Acquisition was done at room temperature (296.9K) for the entire pressure range. **D** values of ^{7}Li are reported in Fig. 11 for IM material Rev 2.0. Due to the lower magnetic

field experienced by the sample in the fringe of the magnet and the static gradient present, S/N suffered and signal averaging had to be done over long time periods. Attenuation was measured due to diffusion according to Eq. 21, and subsequently analyzed using the time domain intensity of the echo. This was done to counteract the line width limitations of the Varian spectrometer, and avoid interference from post-processing audio filters. Data fitting was done in MatLab, using a least-squares (LS) regression analysis, and demonstrate less than 5% statistical deviation from fits.

5.3 Conclusions

The values of **D** collected demonstrate a generally decreasing diffusion coefficient with increasing applied pressure. This is generally expected as restricting volumetric freedom of the sample is expected to reduce translational freedom of the ^{7}Li ions. This trend however exhibits a surprisingly small dependence on pressure for the IM polymer in comparison to expected behavior for conventional PEO type electrolytes. The value of **D** does not decrease by an order of magnitude over the entire applied range, and in fact saturates at high pressures to a lower limit. This is indicative of low coupling of the ion diffusion mechanism to the polymer segmental motion, as increasing pressure restricts these movements effectively. IM polymer Rev 2.0 is therefore believed to possess a unique and effective diffusion mechanism. The value of ambient pressure diffusion, **D** = 2.2E-11m^2/s is astoundingly high in comparison to other polymer based electrolyte systems [26]. Future addendum to this work will hopefully include measurements of the self-diffusion coefficient at these pressures for a conventional PEO based system in the absence of co-solvents, although such a system has yet to be synthesized for study.

Chapter 6: High Pressure Relaxation of Glycerol-Based Eutectic Solvents

The Department of Energy Office of Science, through the Case Western University Breakthrough Electrolytes for Energy Storage (BEES) program, funded this work. This author is responsible for the HP studies of the system, while Dr. Carla Fraenza and Sahana Bhattacharyya at Hunter College are carrying out FFC characterization. Here only the HP work completed so far shall be discussed, within the present limitations of the experiment.

6.1 Introduction and Sample Preparation

Deep Eutectic Solvents (DESs) are a class of solvents with diverse applications that provide an alternative to conventional IL chemistries. They are of great interest in many electrochemical applications, including in secondary battery electrolyte chemistries. Eutectic refers to the varying concentrations of a constituent salt to change the effective physical properties (such as melting point) of the mixture. While IL systems can also form eutectic solvents by mixing metal halides with organic salts, the relatively high cost of ILs stirs interest in alternative eutectic systems [28]. An alternative chemistry of a eutectic solvent is to combine a polar salt with a hydrogen bond donor, which coordinates with the anion of the salt [27]. In this manner, the physical characteristics of the mixture are tunable similar to IL formed eutectic solvents, but in general the substances used as hydrogen bond donors are far more inexpensive and also ecologically sustainable. Glycerol has become a popular choice for its well-documented hydrogen bonded network properties, and widespread availability. A popular ammonium based salt for eutectic applications, and the salt used in this study, is hydroxyethyltrimethylammonium (choline) chloride.

In this study, deuterated glycerol (glycerol-d8) in which the hydrogen is replaced with deuterium (^{2}H), an isotope of hydrogen, is mixed in varying concentrations with choline chloride. Deuterium behaves identically to hydrogen in chemical structures, only altered by its effective mass. Using this isotopologue of glycerol, NMR studies can selectively study the protons present in choline chloride without background from those present in pure glycerol. Likewise, deuterium (I=1) can be selected in NMR studies to study glycerol behavior. Samples of 33% Molar concentration choline chloride (ChCl) mixtures with glycerol-d8 were created at Hunter College by Dr. Carla Fraenza and Sahana Bhattacharyya by solvation in a gentle heat bath. Samples were then pipetted into polyethylene HP-NMR bags cylindrical in shape, and the HP-NMR probe reassembled around the sample. Commercially available pure glycerol and glycerol-d8 were packed in HP bags in an argon glovebox.

6.2 Experimental Details and Results

HP measurements were done at 11T (500MHz) in the homogenous field, at room temperature (296.5K). Measurements were also done for pure non-deuterated glycerol at the same pressures. Both ^{1}H and ^{2}H studies were conducted for all materials, with the HP-NMR probe retuned to the correct Larmor frequency between measurements by switching capacitors. T_1 values were measured using an inversion recovery sequence as demonstrated in Fig. 5 with pressures of [0-240]MPa in increments of 20MPa. All inversion recovery curves were fit in MatLab using a LS regression analysis, and errors are for all curves <4% deviation from average value. Figures 12-14 detail T_1 as a function of pressure for all systems.

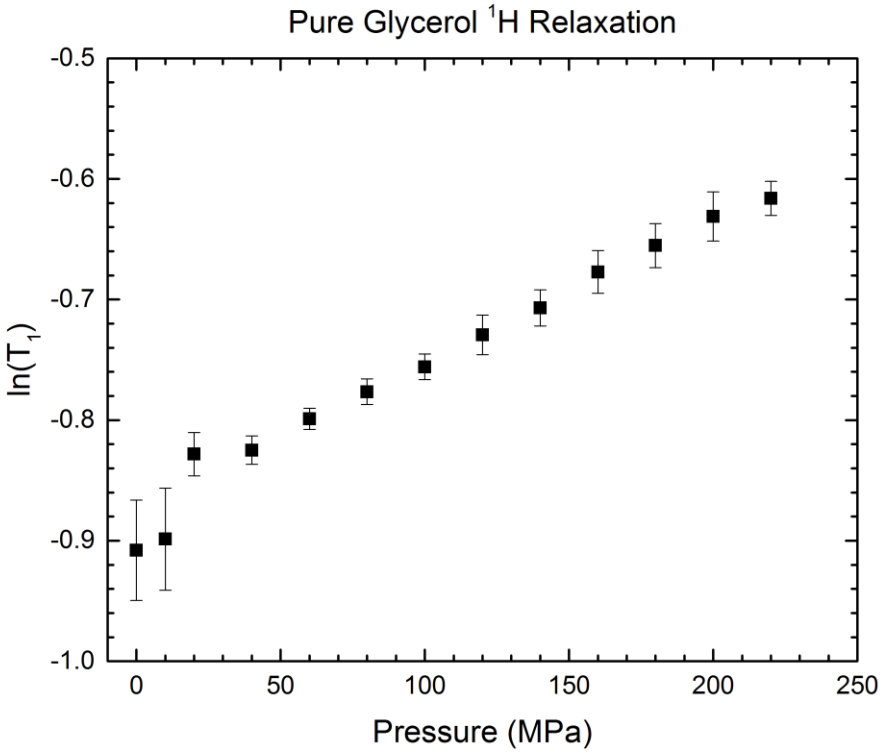

Figure 12. ^{1}H Relaxation for pure glycerol at varying pressure.

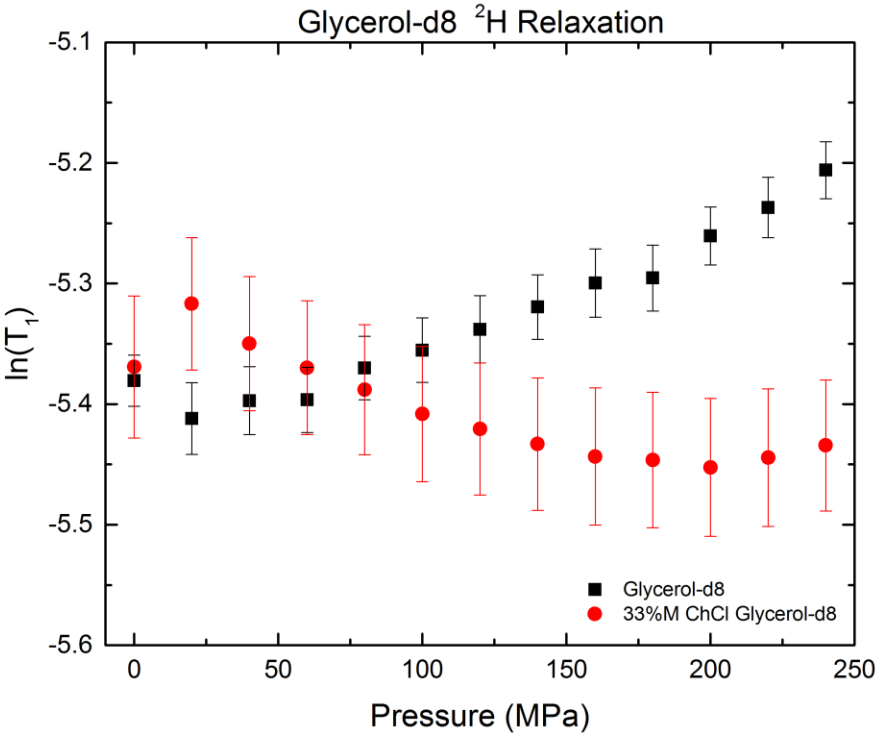

Figure 13. ^{2}H Relaxation for Glycerol-d8, with and without Choline Chloride salt at varying pressure.

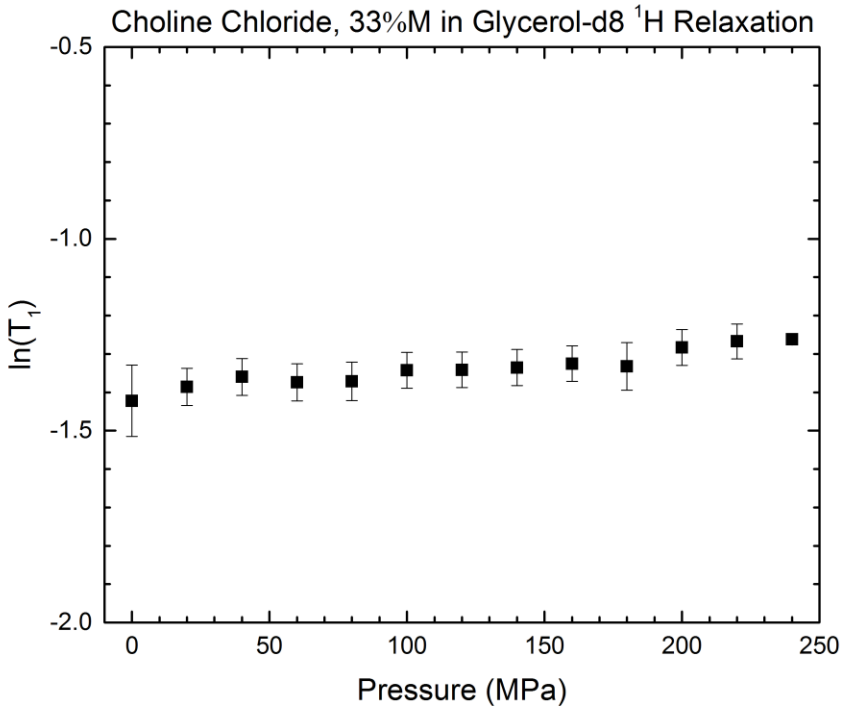

Figure 14. ^{1}H Relaxation for Choline Chloride 33%M mixture in Glycerol-d8, at varying pressure.

6.3 Conclusions

Although HP-NMR data is presented here for several systems, this study is not yet experimentally complete. Analysis of FFC measurements will be supplemented by the HP-NMR data shown here and will be subsequently submitted for publication in the near future. Therefore, only a brief discussion of the behavior revealed by these HP-NMR results will be given here, and the reader is encouraged to see the future publication on the full characterization of these materials from a multi-faceted NMR study.

Fig. 12 demonstrates a generally increasing of ^{1}H T_1 with pressure in pure glycerol, indicating that the relaxation pathways mediated through hydrogen dipolar coupling in the

glycerol network are restricted at higher pressures. This is also seen in the ^2H T_1 values for pure glycerol-d8, with roughly the same reasoning provided. The ^2H T_1 studies of glycerol-d8 in the presence choline chloride reveal a completely different trend, whereby T_1 decreases drastically at higher pressures and appears to saturate in the region >150MPa. This can be interpreted as the polar salt disrupting the hydrogen-bonding network of glycerol, allowing for coupling with the salt to mediate relaxation phenomena. As pressure increases and the intermolecular distances reduce, the coupling between the two chemical species becomes stronger, producing a smaller relaxation time. More careful analysis of FFC relaxation data, particularly in temperature extremes, may validate this conclusion, and reveal sub-leading interactions present in the system. Fig. 14 demonstrates a generally low dependence of ^1H relaxation for choline cations on pressure, perhaps an indication that the polar salt is not heavily dependent on translational motion for its dipolar relaxation modes.

Effectively, choline chloride has been shown through HP-NMR relaxation studies to significantly disrupt the hydrogen-bonded network of glycerol. The effects of the polar salt on physical properties of the system (such as freezing point) are not presented here, but concentration effects on solvent properties will be detailed in later work. High pressure regimes reveal a low dependence of salt relaxation times on intermolecular distances, which requires further study, perhaps in the form of PFG diffusion studies. The ^2H relaxation data presented for both the pure glycerol-d8 and choline chloride mixture demonstrate significant contrasting effects of dipolar interactions with the hydrogen network of glycerol.

References

[1] P. Horowitz, W. Hill, *The Art of Electronics*, Third Edition, Cambridge Univ. Press, Cambridge, 1980.

[2] Hailin Zhang,a Hongbin Zhao, Muhammad Arif Khan, Wenwen Zou, Jiaqiang Xu, Lei Zhangab and Jiujun Zhang. *Recent progress in advanced electrode materials, separators and electrolytes for lithium batteries*. J. Mater. Chem. A, 6, 20564, 2018.

[3] Languang Lu, Xuebing Han, Jianqiu Li, Jianfeng Hua, Minggao Ouyang, *A review on the key issues for lithium-ion battery management in electric vehicles*. Journal of Power Sources 226, 272-288, 2013.

[4] Seungho Yu and Donald J. Siegel, *Grain Boundary Softening: A Potential Mechanism for Lithium Metal Penetration through Stiff Solid Electrolytes* ACS Applied Materials & Interfaces, 10 (44), 38151-38158, 2018.

[5] Seong Jin An, Jianlin Li, Claus Daniel, Debasish Mohanty, Shrikant Nagpure, David L. Wood, *The state of understanding of the lithium-ion-battery graphite solid electrolyte interphase (SEI) and its relationship to formation cycling*, Carbon,Volume 105, 52-76, 2016.

[6] Rabi, I.I.; Zacharias, J.R.; Millman, S. & Kusch, P. *A New Method of Measuring Nuclear Magnetic Moment*. Phys. Rev. 53, (4): 318–327, 1938.

[7] J. D. Jackson, *Classical Electrodynamics*, Third Edition, Wiley, 1999.

[8] E. Fukushima, S. B.W. Roeder, *Experimental Pulse NMR: A Nuts and Bolts Approach*, Westview Press, 1981.

[9] Bloch, F. *Nuclear Induction*. Phys. Rev. 70, 460–474, 1946.

[10] R. Kimmich, *NMR, Tomography, Diffusometry, Relaxometry*. Springer, 1997.

[11] N. Bloembergen, E. M. Purcell, R. V. Pound, *Relaxation Effects in Nuclear*

Magnetic Resonance Absorption, Phys. Rev. 73, 7, 679-712, 1948.

[12] A. Abragam, *The Principles of Nuclear Magnetism*, Oxford Clarendon Press, 1961.

[13] E. O. Stejskal, J. E. Tanner, Spin Diffusion Measurements: Spin Echoes in the Presence of a Time-Dependent Field Gradient. The Journal of Chemical Physics, 42, 288-292, 1965.

[14] 3M Flourinert™ Electronic Liquid FC-40. 3M, St. Paul, Minnesota. 2010.

[15] K. Pilar, *Investigation of Novel Electrolytes for Use in Lithium-Ion Batteries and Direct Methanol Fuel Cells*. Graduate Center, City University of New York, 2018.

[16] R. Kimmich, E. Anoardo, *Field-cycling NMR relaxometry,* Progress in Nuclear Magnetic Resonance Spectroscopy 44, 257-320, 2004.

[17] F. Noack, *NMR Field Cycling Spectroscopy: Principles and Applications,* Progress in NMR Spectroscopy: 18, 171-276, 1986.

[18] R. Kimmich, *Field Cycling NMR Relaxometry,* Bull. Mag. Reson. : 1, N 4, 195, 1980.

[19] Kruk, D., Meier, R., Rachocki, A., Korpała, A., Singh, R. K., Rössler, E. A., *Determining diffusion coefficients of ionic liquids by means of field cycling nuclear magnetic resonance relaxometry*. J. Chem. Phys. 140 (24), 244509, 2014.

[20] J. B. Goodenough and Y. Kim, *Challenges for Rechargeable Li Batteries,* Chem. Mat., 22, 587, 2010.

[21] M. Galinski, A. Lewandowski, and I. Stepniak, *Ionic Liquids as Electrolytes,* Electrochim. Acta, 51, 5567, 2006.

[22] Kartik Pilar.; Armando Rua.; Sophia N. Suarez.; Christopher Mallia.; Shen Lai.; J. R. P. Jayakody.; Jasmine L. Hatcher.; James F. Wishart.; Steve Greenbaum. *Investigation of Dynamics in BMIM TFSA Ionic Liquid through Variable Temperature and Pressure NMR Relaxometry and Diffusometry*. Journal of The Electrochemical Society, 2017 164 (8) H5189-H5196.

[23] O. Borodin, W. Gorecki, G. D. Smith, and M. Armand, *Molecular dynamics simulation and pulsed-field gradient NMR studies of bis(fluorosulfonyl)imide (FSI) and bis[(trifluoromethyl)sulfonyl]imide (TFSI)-based ionic liquids*, J. Phys. Chem. B, 114, 6786, 2010.

[24] S. N. Suarez, A. Ru´a, D. Cuffari, K. Pilar, J. L. Hatcher, S. Ramati, and J. F. Wishart, *Do TFSA Anions Slither? Pressure Exposes the Role of TFSA Conformational Exchange in Self-Diffusion*, J. Phys. Chem. B, 119, 14756, 2015.

[25] T. C. Penna, L. F. O. Faria, J. R. Matos, and M. C. C. Ribeiro, *Mechanical heterogeneity in ionic liquids*, J. Chem. Phys., 138, 104503, 2013.

[26] S. Munoz, *NMR Characterizations of Candidate Battery Electrolytes Graduate Center*, City University of New York, 2018.

[27] A.P. Abbott, G. Capper, D.L. Davies, R.K. Rasheed, V. Tambyrajah, *Novel solvent properties of choline chloride/urea mixtures*, Chem. Commun. 70–71, 2003.

[28] Mohamed Khalid AlOmar, Maan Hayyan, Mohammed Abdulhakim Alsaadi, Shatirah Akib, Adeeb Hayyan, Mohd Ali Hashim, *Glycerol-based deep eutectic solvents: Physical properties*, Journal of Molecular Liquids, 215, 98-103, 2016.

Appendix A

Table 1. 1H R_1 values measured via FFC for various temperatures and frequencies. Values are in s^{-1}

	Temperature (K)														
Field (MHz)	263	268	273	278	283	288	293	298	303	308	313	318	323	328	333
35	9.33	9.09	8.10	8.07	8.34	7.57	5.60	3.69	3.12	2.84	2.53	2.27	2.05	1.88	1.07
23.04	15.54	14.97	13.99	12.68	10.96	9.36	7.27	3.99	3.47	3.03	2.65	2.36	2.23	1.92	1.06
15.16	21.81	20.67	19.07	16.35	13.97	11.22	8.96	4.33	3.71	3.16	2.79	2.37	2.17	1.95	1.09
9.98	25.91	25.65	22.42	18.90	15.39	13.05	10.21	5.06	4.31	3.68	3.14	2.95	2.57	2.29	1.37
6.56	33.16	30.99	26.81	22.16	17.75	14.46	11.35	5.19	4.45	3.76	3.18	2.86	2.44	2.30	1.33
4.32	38.64	35.07	30.93	24.44	19.40	15.41	12.12	5.23	4.48	3.83	3.28	2.87	2.54	2.24	1.27
2.84	44.49	38.74	34.50	26.44	20.58	16.44	12.39	5.32	4.56	3.85	3.33	2.90	2.55	2.22	1.26
1.87	48.62	41.64	36.58	27.94	21.62	17.02	13.14	5.46	4.57	3.95	3.35	2.87	2.51	2.23	1.25
1.23	50.93	45.16	38.44	28.96	22.59	17.20	13.39	5.42	4.58	3.92	3.30	2.86	2.48	2.26	1.26
0.81	54.10	46.72	40.42	29.85	23.20	17.81	13.62	5.55	4.64	3.86	3.34	2.93	2.52	2.25	1.25
0.53	56.61	48.59	41.41	30.97	23.82	18.47	14.11	5.49	4.61	3.95	3.38	2.90	2.48	2.22	1.25
0.35	58.52	49.55	43.46	31.90	23.83	18.65	14.31	5.59	4.68	3.92	3.41	2.90	2.55	2.23	1.26
0.23	59.88	49.50	44.73	32.26	24.80	18.60	14.39	5.54	4.65	3.97	3.32	2.93	2.56	2.27	1.26
0.15	61.81	51.19	44.98	32.38	24.24	18.84	14.61	5.58	4.69	3.92	3.32	2.93	2.55	2.25	1.26
0.1	62.65	51.79	45.40	33.10	25.25	18.98	14.69	5.77	4.81	4.01	3.39	2.97	2.59	2.28	1.29